



King Saud University
Arabian Journal of Chemistry

www.ksu.edu.sa
www.sciencedirect.com



ORIGINAL ARTICLE

In-vitro cytotoxicity evaluation of surface design luminescent lanthanide core/shell nanocrystals



Anees A. Ansari^{a,*}, Shahanavaj Khan^b, Ali Aldalbahi^a, Abdul K. Parchur^c,
B. Kumar^c, Ashok Kumar^d, Mohammad Raish^e, S.B. Rai^c

^a King Abdullah Institute for Nanotechnology, King Saud University, Riyadh 11451, Saudi Arabia

^b Nanomedicine & Biotechnology Research Unit, Department of Pharmaceutics, College of Pharmacy, PO Box 2457, King Saud University, Riyadh 11451, Saudi Arabia

^c Department of Physics, Banaras Hindu University, Varanasi 221005, India

^d Vitiligo Research Chair, College of Medicine, King Saud University, Riyadh 11451, Saudi Arabia

^e Department of Pharmaceutics, College of Pharmacy, King Saud University, Riyadh 11451, Saudi Arabia

Received 13 September 2017; accepted 29 October 2017

Available online 11 November 2017

KEYWORDS

Core/shell/SiO₂NCs;
Toxicity;
Absorption spectra;
Optical band gap;
Luminescent property

Abstract Lanthanide nanocrystals (NCs) are the most promising luminescent materials for bioapplications, but their use is hindered by difficulties in obtaining biocompatible and photoluminescence lanthanide NCs. To solve this problem, a simple and versatile strategy was developed for improving the luminescence efficiency with the hydrophilicity of the lanthanide NCs. In this study, the effects of shell formation on structural, morphological, and optical properties (optical absorption, band-gap energy, excitation, emission, and luminescent decay time) were evaluated. To improve the luminescence efficiency and aqueous dispersion, luminescent core-NCs were encapsulated with inert NaGdF₄ and amorphous silica layers. These surface coating layers significantly improved the luminescence efficiency and dispersion of the core/shell NCs in which the silica surface provides a negatively charged surface to the NCs at physiological pH. Optical properties of these NCs strongly depend on the external change of NCs, demonstrating the impact of coating in improving the luminescence efficiency. The outcomes can be ascribed to the development of surface chemical bonds between core/shell and noncrystalline SiO₂ shell via Gd—O—Si bridges, activating the ‘dormant’ Ce³⁺ and Tb³⁺ ions on the surface of NCs. An intensive emission and good hydrophilic property from the active functional groups in solutions show a great potential for

* Corresponding author.

E-mail address: aneesaansari@gmail.com (A.A. Ansari).

Peer review under responsibility of King Saud University.



Production and hosting by Elsevier

applications such as multi-analyte fluorescent biolabeling, optical biosensing, staining, display, and other optical technologies. The core/shell/SiO₂ NCs showed higher nontoxicity and biocompatibility with respect to the core NCs because of biocompatible silica surface modification, facilitating entry into the living cells. Therefore, this developed synthesis approach might advance the field of biomolecule-based nanotechnology in near future.

© 2017 Production and hosting by Elsevier B.V. on behalf of King Saud University. This is an open access article under the CC BY-NC-ND license (<http://creativecommons.org/licenses/by-nc-nd/4.0/>).

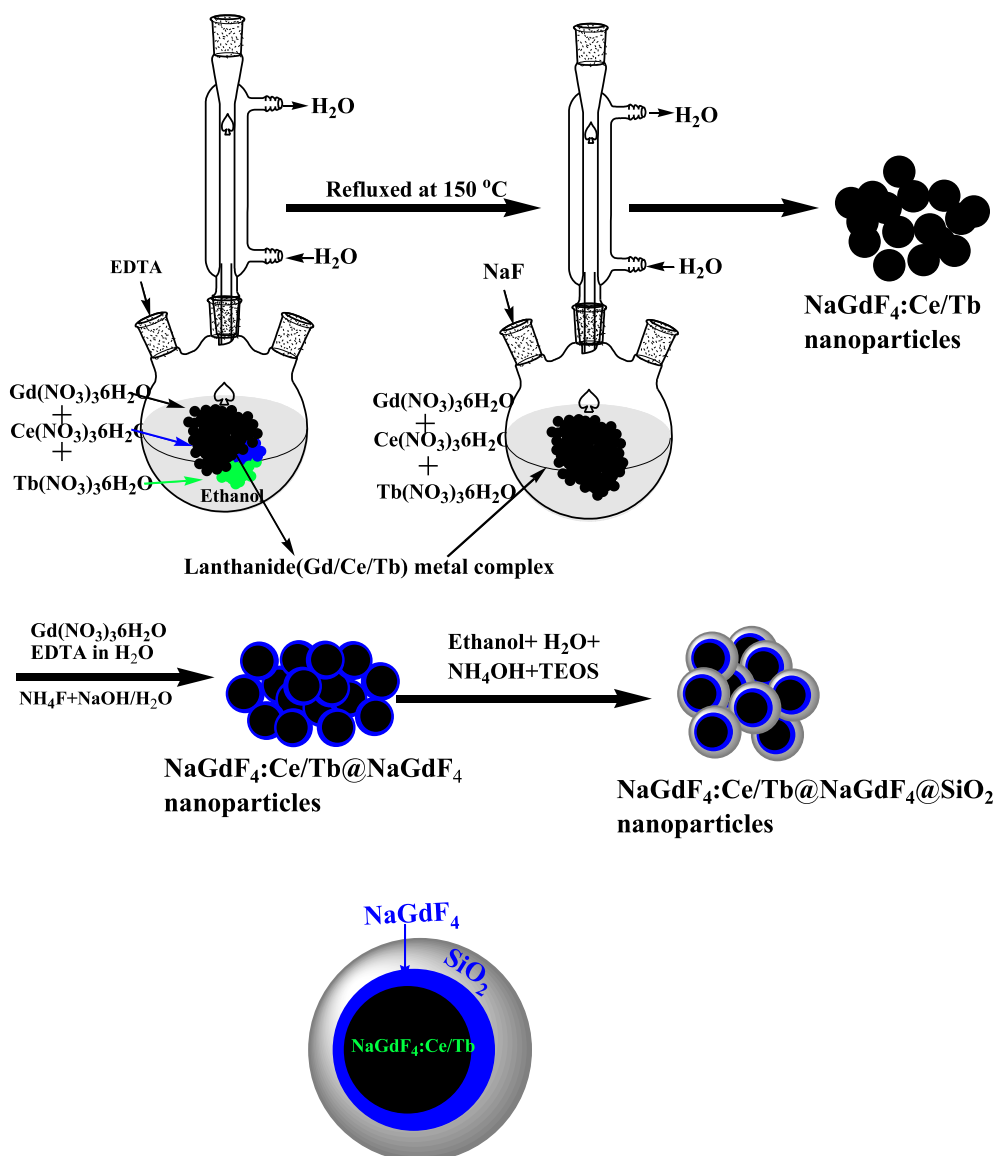
1. Introduction

Presently, luminescent ion-doped lanthanide nanomaterials have fascinated much interest in diverse life science applications owing to their narrow and strong $f-f$ emission transitions, longer luminescence lifetimes, high quantum yields, large effective Stokes shifts, and tunable multicolor emissions (Huhtinen et al., 2005; Ansari et al., 2011; Parchur et al., 2012). Compared to traditional organic fluorophores, luminescent latex/silica nanobeads and quantum dots used in bioimaging and bio-detection, trivalent lanthanide ion-doped NCs show superior properties such as a high chemical stability, high resistance to photobleaching blinking and photochemical degradation, excellent biocompatibility, and low toxicity (Alivisatos, 2004; Liu et al., 2005; Reiss et al., 2009). In addition, luminescent materials in nanoparticle form have several advantages over the corresponding larger or micron-sized particles. Luminescent materials such as lanthanide ion-doped Y₂O₃ nanoparticles show a higher luminescence in respect to their macro-sized materials under ultraviolet excitation. This can be attributed to the enhancement in energy band gap with reduced in the particle size of the host matrix (Y³⁺-O²⁻), thus increasing the absorption cross-section of NCs (Dhanaraj et al., 2001). Energy transfer from the host to lanthanide ion is higher for the NCs than the bulk (Wang et al., 2011). Moreover, the maximum lanthanide ion emission does not change. Therefore, extensive studies have been reported on NCs doped with lanthanide ions (Riwotzki et al., 2000; Goldys et al., 2006; Wang et al., 2011). These useful properties of luminescent lanthanide NCs make them an ideal target material for fluorescent biolabeling, optical probes, and drug-delivery systems.

Among different host materials, lanthanide-doped NCs such as sodium gadolinium fluoride (NaGdF₄) have some distinct advantages over the conventional oxide nanomaterials because of very low phonon frequencies, high refractive index, and tunable crystal phase (Zhang et al., 2005; Vetrone et al., 2009; Kar et al., 2015). Quenching of the excited state of lanthanide ions is minimized when the ions are doped into fluoride hosts, leading to long lifetimes of their excited states and high luminescence quantum yields. Furthermore, Gd³⁺ acts as an intermediate to distribute the excited energy over the Gd³⁺ sub-lattice, thus facilitating energy transfer (Vetrone et al., 2009). NaGdF₄ crystal has been shown as the most efficient host lattice for such luminescent materials. Boyer et al., prepared Ce and Tb-doped NaGdF₄ NCs; they formed colloidal solutions in nonpolar organic solvents (Boyer et al., 2007). Chen and co-workers prepared phase-controlled NaGdF₄ NCs with monodispersed morphology, exhibiting an intense multicolor luminescence invisible region (Liu et al., 2009). Wang et al., reported a one-pot hydrothermal procedure for the synthesis of multicolor colloidal poly-

ethyleneimine capped NaGdF₄:Ce, Ln (Tb, Eu, Sm, and Dy) NCs (Wang et al., 2007). Generally, surface capping agents such as surfactants and organic moieties or ligands affect the luminescence intensity because of the occurrence of several surface effects such as a large specific surface area, lattice distortion, broken bonds, surface adsorption, and other surface defects. These enhance the nonradiative transitions and scatter the excitation irradiation of luminescent NCs, and even significantly decrease the emission intensity. To overcome this problem and improve the overall photoluminescence efficiency of lanthanide ion-doped NCs, core/shell heterostructures have been prepared (Parchur et al., 2012; Ansari et al., 2014a, 2014b). Addition of an inert inorganic shell surrounding the core-NCs significantly improved the luminescence efficiency of a core/shell heterostructure, because the inert shell protects the luminescent dopant ions and prevents the defect sites on the particle surface from luminescence quenching caused by the surrounding environment (e.g., stabilizing ligands, solvent molecules, and surface defects) (Wang et al., 2006; Boyer et al., 2007). Owing to the inert shell surface of the lanthanide ion-doped NCs, their colloidal dispersion in an aqueous solvent decrease, limiting their applications in biological sciences. To improve their performance in biological sciences, several studies have been conducted to enhance their properties (biocompatibility, water dispersion, and nontoxicity) and surface area's area; new functionalities have been introduced by combining them with other functional nanomaterials (Wang et al., 2007; Liu et al., 2009; Ansari et al., 2011; Kang et al., 2011; Ansari and Labis 2012; Bao et al., 2012; Cui et al., 2012; Ansari et al., 2013; Xu et al., 2013). Amorphous silica surface coating is a convenient strategy obtained through the hydrolysis or hydrothermal condensation of triethyl orthosilicate; the so-called core/shell structure can solve this problem. This is very important for their biological applications (Tauc and Menth, 1972; Ansari et al., 2012).

Here, we report the synthesis of Ce³⁺ and Tb³⁺-doped NaGdF₄ (core) NCs that can be dispersed as colloidal solutions in aqueous solvents. To improve their luminescence efficiency and colloidal stability in aqueous solvents, we modified the surface of core-NCs with an inert inorganic shell and amorphous silica layers. Structural and optical properties of the core, core/shell, and silica surface modified core/shell NCs were compared to evaluate the effects of surface coating surrounding the core NCs under UV excitation. The results indicate that the luminescence intensities of Ce and Tb co-doped NaGdF₄ core-NCs in the inert shell core/shell structures significantly enhanced. Compared to the inert shell-coated NCs, luminescence intensities of the amorphous silica layer deposited core/shell NCs significantly decreased. Owing to the inert shell formation prior to the silica layer deposition around the core-NCs, they showed better performance than the silica surface



Scheme 1 Schematic illustration for the synthesis of core, core/shell and core/shell/SiO₂ NCs through general synthesis approach.

modified core/shell NCs reported in the literature. Therefore, more intense green luminescence with high radiative quantum efficiencies enables SiO₂-coated Ce³⁺ and Tb³⁺-doped core-NCs as a fine resolution phosphor. Moreover, the possible cytotoxic response and entering efficiency of the synthesized NaGdF₄:Ce³⁺/Tb³⁺@NaGdF₄ (core/shell) and NaGdF₄:Ce³⁺/Tb³⁺@NaGdF₄@SiO₂ (core/shell/SiO₂) NCs in HT-29 cells were also evaluated through an *in vitro* study.

2. Experimental

2.1. Materials

Gadolinium oxide (99.9% BDH Chemicals, UK), Ce(NO₃)₃·6H₂O (BDH Chemicals, UK), terbium oxide (99.9% Alfa Aesar, Germany), ethylenediamine tetraacetic acid (EDTA), NaF, ammonia, ethanol, NaOH, HNO₃, SiC₈H₂₀O₄ (TEOS, Analytical grade) were analytical grade and used directly as received

without any further purifications. Gd(NO₃)₃·6H₂O and Tb(NO₃)₃·6H₂O were prepared by dissolving respective metal oxides into diluted nitric acid. Milli-Q (Millipore, Bedford, USA) water was used for synthesis and characterization.

2.2. Synthesis of NaGdF₄:Ce/Tb (Core) NCs

Ce³⁺ & Tb³⁺-doped NaGdF₄ NCs was prepared at ambient condition (~150 °C) using EDTA as a chelating agent. Freshly prepared equal molarity solution of Gd(NO₃)₃·6H₂O, Ce(NO₃)₃·6H₂O and Tb(NO₃)₃·6H₂O in 9:0.5:0.5 mL ratio was mixed together in absolute ethanol and heated up to 80 °C. Then an aqueous dissolved EDTA solution in 1:1 M ration solution was injected into the foregoing reaction for complex formation with metal ions. After complete homogenization aqueous dissolved 0.627 g sodium fluoride was added slowly to the vigorously stirred solution mixture. This solution mixture was heated up under a refluxed condition at 150 °C for

3 h (Zhang et al., 2005). Occurred precipitate was separated by centrifugation and washed with ethanol and distilled water, later dried at 80 °C in the oven for further characterization. Similar method was applied for synthesis of NaGdF₄:Ce³⁺/Tb³⁺@NaGdF₄ (core/shell) NCs.

2.3. Synthesis of NaGdF₄:Ce/Tb@NaGdF₄/SiO₂ (core/shell/SiO₂) NCs

A versatile Stober based sol-gel process was employed for synthesis of silica modified NaGdF₄:Ce/Tb@NaGdF₄@SiO₂(core/shell/SiO₂) NCs (Ansari et al., 2012; Ansari et al., 2014a, 2014b). As-prepared core/shell NCs were dispersers with the help of ultrasonication for half-an-hour in a minimum amount of dist. water. After that they centrifuged and further dispersed in a solution containing 50 mL water, 70 mL ethanol and 1 mL liquid ammonia for 30 min under mechanical stirring at room temperature. After that 1 mL, TEOS was injected slowly into the vigorously stirred solution, and whole solution mixture was allowed to proceed for continuous mechanical stirring at room temperature for 5–6 h. Occurred precipitate was centrifuged and washed with ethanol and dist. water, later dried in an oven at 80 °C for further characterization (Scheme 1).

2.4. Characterizations

Powder X-ray diffraction (XRD) pattern was carried out by using PANalytical X'Pert X-ray diffractometer equipped with Ni filter and CuK α ($\lambda = 1.5405 \text{ \AA}$) radiations. Morphological micrographs were taken from Field emission -transmission electron microscope (FE-TEM, JEM-2100F, JEOL, Japan) equipped with energy dispersive X-ray analysis (EDX), operating at an accelerating voltage of 200 kV. Infrared spectra were obtained from Perkin-Elmer 580B IR spectrometer using KBr pellet technique. Optical absorption spectra were recorded on Carry 60 UV/Visible spectrophotometer (Agilent Technologies, USA) in UV/Visible region. Photoluminescence spectra were measured by Perkin-Elmer photoluminescence spectrophotometer equipped with Xenon lamp as an excitation source.

2.5. Cell culture and potential cytotoxicity

HT-29 cell line (human colon carcinoma) was cultured in DMEM containing antibiotics such as ~100 mg/mL streptomycin, 100 units/mL penicillin, and 10% BSA in a humidified incubator supplied with 5% CO₂ and 95% air at 37 °C. The confluency of the cell was maintained about 70 % prior to experiments. In experiments, 24 h after splitting, there was a starvation phase by changing the used medium with fresh medium.

2.5.1. Preparation of different serial concentrations of synthesized NCs samples

Various serial diluted concentrations of core and core/shell/SiO₂ NCs suspensions (3.12, 6.25, 12.5, 25, 50, and 100 $\mu\text{g/mL}$) were prepared in distilled water. The different concentrations of doxorubicin were used as control drug as our recently published article (Khan et al., 2016a, 2016b).

2.5.2. MTT assay for estimation of cytotoxic response of core NCs

To assess the cytotoxic response of core NCs on the viability of growing cell, MTT reduction assay was performed against HT-29 cell line. Briefly, the HT-29 cell line was maintained in regular medium. About 70 % confluence cells were split and transfer into 96 well plates with an average density of 5×10^3 cells per well. Six serial dilutions of test sample were used in experiments. After 24 h, 100 μL of the medium was aspirated and an equal volume of different concentrations of core NCs (equivalent to 3.12, 6.25, 12.5, 25, 50, and 100 $\mu\text{g mL}^{-1}$) has been added to each well. The experiments were performed in triplicate. The MTT assay was performed after 24 h according to our recently published reports (Khan et al., 2016a, 2016b).

2.5.3. MTT assay for estimation of cytotoxic response of core/shell/SiO₂ NCs

Also, to assess the cytotoxic response of core/shell/SiO₂ NCs on the viability of growing cell, MTT reduction assay was performed against HT-29 cell line. Briefly, the HT-29 cell line was maintained in regular medium. About 70 % confluence cells were split and transfer into 96 well plates with an average density of 5×10^3 cells per well. Six serial dilutions of test sample were used in experiments. After 24 h, 100 μL of the medium was aspirated and equal volume of different concentrations of core/shell/SiO₂ NCs (equivalent to 3.12, 6.25, 12.5, 25, 50, and 100 $\mu\text{g/mL}$) has been added to each well. The experiments were performed in triplicate. The MTT assay was performed after 24 h according to our recently published reports (Khan et al., 2015; Khan et al., 2016a, 2016b).

2.5.4. Estimation of value of IC₅₀ (half maximal inhibitory concentration)

The IC₅₀ in term of percent inhibition of viability of cells for every concentration of the core and core/shell/SiO₂ NCs were calculated and compared to the control. The average of three experiments for each concentration was used to evaluate the value of IC₅₀.

2.6. Invert microscopy for analysis of morphological alterations in HT-29 cell line

Any possible alterations in the morphology of growing HT-29 cell line were analyzed by inverted microscopy with untreated control cells. The growing HT-29 cells were treated with 100 $\mu\text{g/ml}$ concentration of core and core/shell/SiO₂ NCs in distinct experiments along with untreated control groups for 24 h. Crystal violet staining was performed to observe any potential changes in morphology of HT-29 cells as our previous studies (Khan et al., 2016a, 2016b).

3. Results and discussion

3.1. Crystal structure and morphology

To confirm the formation of nanostructures and possible phase change during the synthesis process XRD patterns were recorded. The XRD patterns in Fig. 1 depicts all the possible characteristic peaks of core, core/shell and core/shell/SiO₂

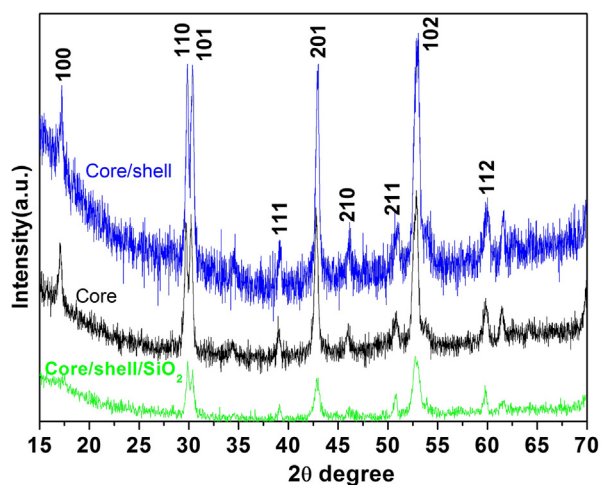


Fig. 1 X-ray diffraction pattern of core, core/shell and core/shell/SiO₂ NCs.

NCs, which are well matches with **JCPDS card No.27-0699**. These sharp XRD patterns indicated that the core, core/shell, and core/shell/SiO₂ NCs having hexagonal phase structure and high crystallinity. Moreover, no additional impurity phases were observed in XRD pattern, confirming the phase purity and homogeneously distribution of Ce³⁺ and Tb³⁺ ions into the NaGdF₄ host. Furthermore, the intensity of XRD patterns of the core/shell NCs is slightly higher than core NCs (Fig. 1). This is may be due to increase grain size and crystallinity after NaGdF₄ shell formation around core. The diffraction peaks at angle 2θ, 17°, 29°, 42°, and 52° corresponding to (1 0 0), (1 1 0), (2 0 1), and (1 0 2) planes, respectively. It is worth noticing that, the intensity of diffraction patterns after silica modified core/shell/SiO₂ NCs are lower than both core and core/shell NCs. Which confirms the formation of thin amorphous silica shell around core/shell NCs. Nevertheless, owing to the thinner silica layer over the core/shell NCs no well-defined silica peak is detected in XRD pattern. It suggests that SiO₂ coating significantly influences the grain size, resulting from the alteration in diffraction peak intensity of XRD pattern. Due to a lot of noise in the XRD patterns it is difficult to calculate the exact XRD patterns peak position and its broadening to calculate the unit cell volume and crystallite size. Furthermore, the increase in NCs size due to shell formation is confirmed using TEM study.

TEM micrographs were carried out to examine the shape and size of the as-fabricated core and surface silica modified core/shell/SiO₂ NCs. TEM photographs in Fig. 2 obviously demonstrate the good crystallinity of NCs. Core-NCs are in irregular spherical shape, monodispersed and well-defined size distributions with a particle size of ~102–152 nm and core/shell/SiO₂ NCs are ~165 nm. Selected area electron diffraction (SAED) pattern verified the hexagonal crystal matrix of the as-designed host materials (inset in Fig. 2a). The rings of the SAED pattern arises from different planes of the standard hexagonal NaGdF₄ structure (JCPDS 27–0699) (Wang et al., 2007; Liu et al., 2009). Fig. 2a revealed diffraction ring in SAED pattern are ascribed to the (1 1 1), (2 0 0), (2 2 0), (3 1 1), (4 0 0) and (3 3 1) planes of the hexagonal NaGdF₄ crystal lattice (Wang et al., 2007). As observed from Fig. 2b, the distance between the lattices fringes is measured to be 3.1 Å,

which attributed to the d-spacing for the (1 1 1) crystal lattice plane of the cubic NaGdF₄ structure. The core NCs with subsequent layers of NaGdF₄ and SiO₂ shells results in the increase in nanoparticle size, which confirmed the formation of layers over the seed core-NCs. The thickness of core/shell NCs amplified up to 10–15 nm for NCs with both NaGdF₄ and SiO₂ shells. Fig. 2c–e displays the TEM image of gradually undoped NaGdF₄ and silica surface modified core/shell NCs. We and previously some researchers observed that, due to the similar crystal structure and the reflective index of the core and insulating shell, it is difficult to accurately determine the thickness of undoped coated layer (Wang et al., 2011; Parchur et al., 2012; Prorok et al., 2014; Ansari et al., 2016). These core/shell NCs are hydrophobic in nature, because of the exterior crystalline inert NaGdF₄ layer, therefore, their solubility in aqueous media and their use in the biological window is limited. It is an urgent need to make them hydrophilic in nature, which can easily conjugate with bio-macro-molecules and show high solubility and colloidal stability in an aqueous environment. Amorphous silica surface modification is an easy, fast and safe method to make them an ideal core/shell materials as per required biomedical applications. Because of different electron penetrability between core and silica modified core/shell NCs, it is easy to distinguish core and shell in the core/shell/SiO₂ nanostructure. As seen in Fig. 2c–e, the dark color is core and light gray color are belong to the silica shell in core/shell/SiO₂ structure. As shown in Fig. 2e, around 10–12 nm amorphous silica layer has been effectively grafted over the core/shell NCs. It is observed that no bare or silica particles are observed in TEM images, it indicated that sol-gel process allows for a homogeneous and complete surface coating over the NCs. Notably, the SAED of core/shell/SiO₂ NCs exhibits diminished spotty polycrystalline diffraction ring patterns corresponding to the specific planes. It is notable that crystal lattice fringes from core NCs are clearly captured in high-resolution TEM micrographs, whereas, lattice fringe in silica surface modified core/shell NCs are diminished (Fig. 2d) and the high crystallization of core-NCs and the amorphous nature of silica layer are confirmed. Additionally, after silica encapsulation surrounding the core/shell-NCs the crystallinity decrease due to amorphous silica nature. EDX analysis was adopted to determine the doping and silica surface coating in the core and core/shell/SiO₂ NCs. The existence of all doping constituents in the core (Na, Gd, F, Ce and Tb) and in surface modified core/shell/SiO₂ (Na, Gd, F, Ce, Tb, O and Si) NCs verified the silica surface coating over the as-designed nanostructured (Fig. 3). The EDX spectrum of core/shell/SiO₂ NCs demonstrate the strong peak at 1.6 eV, it confirmed the successful growth of silica layer. An appearance of strong peaks of C and Cu in the middle of EDX spectra are belonging to the carbon-coated copper grid. No other additional peak is observed in the EDX spectra resulting in the phase purity of the as-synthesized nanomaterials.

Surface chemistry of the synthesized core, core/shell, and silica-coated core/shell NCs were verified by the FTIR spectroscopy. All samples in Fig. 4 show a diffused band in between 3000–3580 cm⁻¹ and a low-intensity band at 1630 cm⁻¹, which is attributed to the asymmetric stretching νOH vibration of H₂O molecules adsorbed on the surface of the NCs (Ansari et al., 2012; Ansari et al., 2014a, 2014b). In Fig. 4 three sharp fragile intensity peaks at 1750, 1400, and 1232 cm⁻¹ are also observed. The observed two peaks at

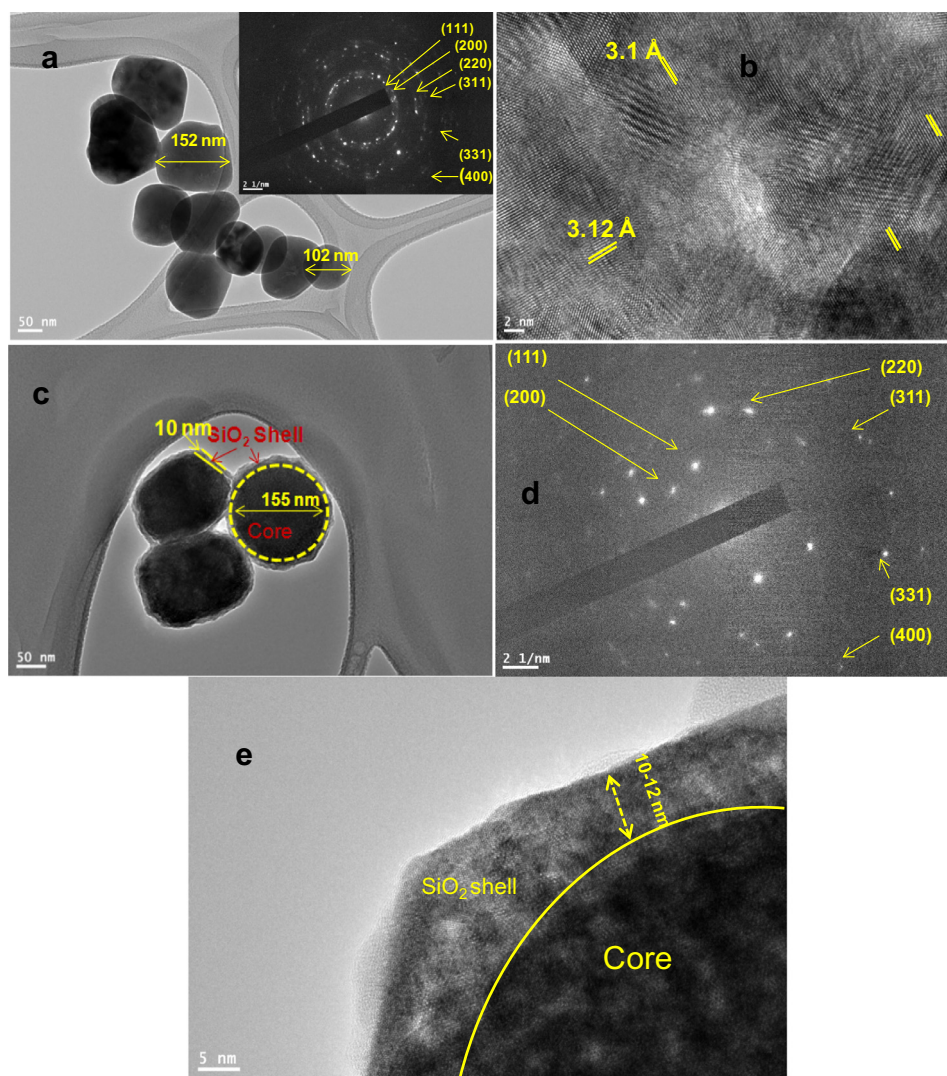


Fig. 2 TEM images of (a&b) core inset shows the SAED pattern (c&e) core/shell/SiO₂ NCs and (d) SAED pattern of core/shell/SiO₂ NCs.

1750, 1400 cm⁻¹ are due to the carboxylic acid (C=O) stretching vibration modes and amino (C=N) modes into the EDTA, while the peak at 1232 cm⁻¹ arises from the C–N stretching vibration. It is observed that after silica surface modification, the intensity of these bands is enhanced. In the case of core/shell/SiO₂ NCs, a strong doublet band at 1236, 1072, and 450 cm⁻¹ also seen, which correspond to the stretching vibrational modes of Si–O, Si–OH and Si–O–Si molecules, respectively (Ansari et al., 2011; Ansari et al., 2012; Ansari et al., 2014a, 2014b). These infrared bands verified that the silica was successfully encapsulated over the surface of core/shell NCs.

Optical absorption spectra were performed to determine the influence of surface coating on optical properties of as-designed nanomaterials. The absorption spectra of these nanomaterials in ethanol illustrate the characteristic absorption band in the ultraviolet region, which is greatly improved in core/shell/SiO₂ NCs, causing the optically active silica surface modification (Fig. 5). Tauc and Menth's method was employed for the determination of energy band gap (E_g) from sharply

increasing absorption region (Tauc and Menth, 1972). As shown in the inset Fig. 5, a plot of $(\alpha h\nu)^2$ versus photon energy ($h\nu$). In the high-energy region of the absorption edge, $(\alpha h\nu)^2$ varied linearly with $h\nu$ and the straight-line behavior in the high-energy region is used as evidence for the direct band gap. The experimentally observed band gap energies are 2.02, 1.799, and 1.43 eV for the core, core/shell, and core/shell/SiO₂ NCs, respectively. It is observed that band gap energy is decreased after an increase the surface coating, it attributed due to increasing the crystalline size of the samples (Ansari et al., 2012; Ansari et al., 2014a, 2014b). These observations are in accord of XRD study, which signified the reduction of reflection peak intensity after shell formation because of decrease crystalline size of the materials.

Photoluminescence spectra were recorded to determine the optical features of the as-designed nanomaterial. The excitation spectra of all three samples were measured on monitoring 541 nm emission wavelength as shown in Fig. 6. The excitation spectra of all three samples exhibit a diffused excitation band located at 250 nm along with some sharp emission transitions

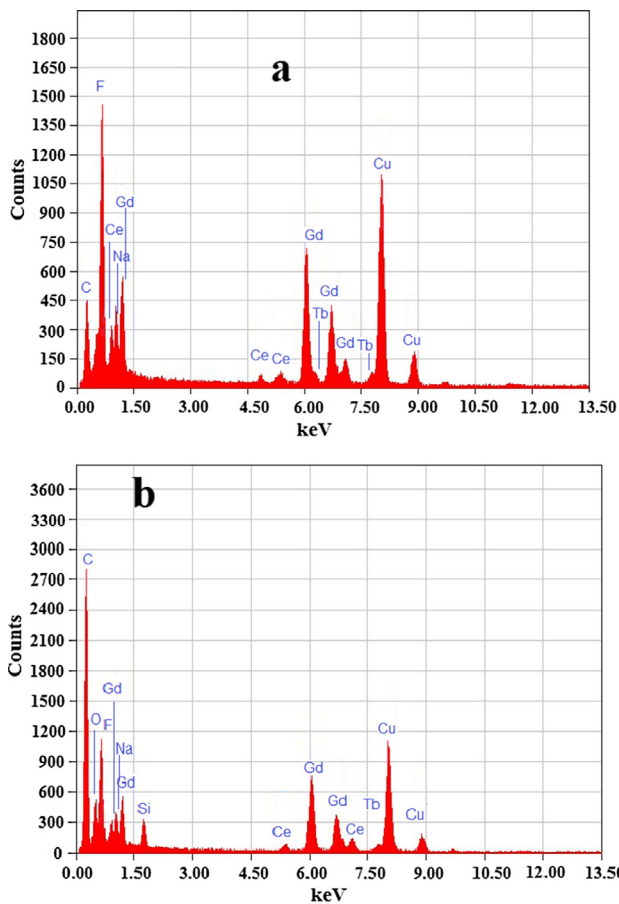


Fig. 3 Energy dispersive X-ray spectrograph core and core/shell/SiO₂ NCs.

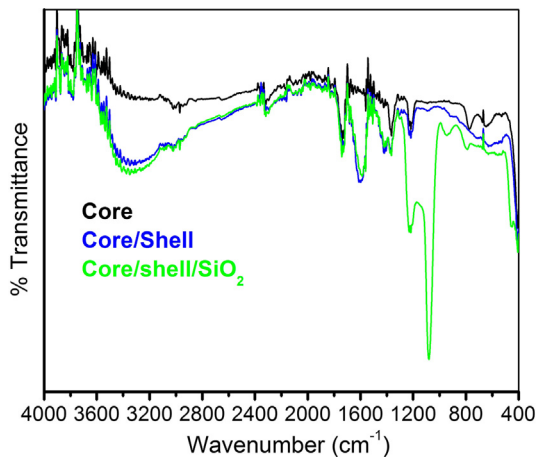


Fig. 4 FTIR spectra of core, core/shell and core/shell/SiO₂ NCs.

in between 300–500 nm. The broadened band is due to the electronic transitions from 5*d* to 4*f* states of Ce³⁺ ions and sharp excitation peaks correspond to the 4*f*-4*f* lines of Tb³⁺ ions. The appearance of another strong transition in all samples at 274 nm corresponds to the ⁸S_{7/2} → ⁶I_{11/2} transition of Gd³⁺, and this transition has the strong absorption in UV region relative to the Tb³⁺ ion transitions (Yaiphaba et al.,

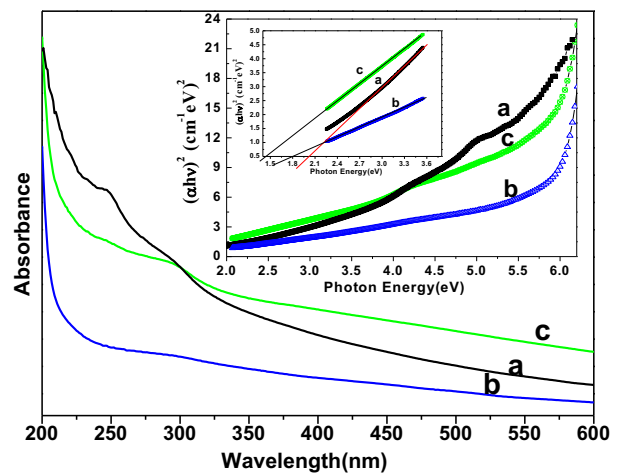


Fig. 5 UV-vis absorption spectra of (a) core (b) core/shell and (c) core/shell/SiO₂ NCs suspended in absolute ethanol inset shows the plot of (αhν)² vs. photon energy (hν) of the (a) core (b) core/shell and (c) core/shell/SiO₂ NCs.

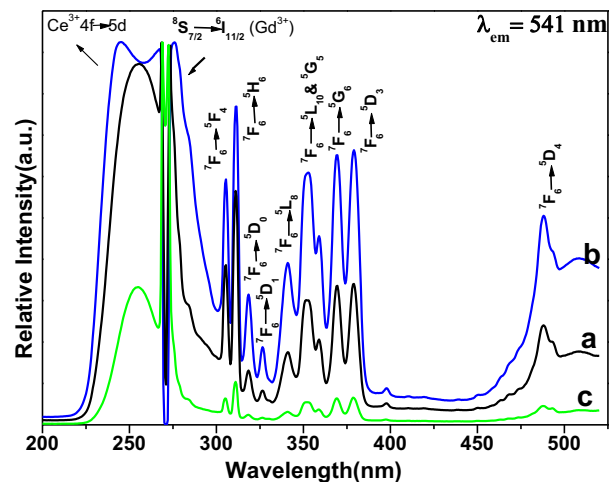


Fig. 6 Excitation spectra of (a) core (b) core/shell and (c) core/shell/SiO₂ NCs.

2010a, 2010b; Parchur et al., 2012; Gao et al., 2015). The occurrence of these excitation transitions indicating the efficient energy transfer process from Ce³⁺ to Gd³⁺ and further luminescent center (Tb³⁺ ion). In view of literature reports, the photoluminescence spectra of lanthanide ions demonstrate mainly two type electronic transitions: first one 4*f*-4*f* and secondly 4*f*-5*d* or (²F_{5/2} → 5*d*) transition (Yaiphaba et al., 2010a, 2010b; Ansari and Labis 2012; Parchur et al., 2012; Ansari et al., 2013, Gao et al., 2015). In which, 4*f*-4*f* transitions are generally narrow emission lines, whereas, 4*f*-5*d* transitions are broadened in character. The 4*f*-4*f* transitions are sharp causing the 4*f*-orbital is covered by the filled 5*s*²*p*⁶ sub-shells. In this case excitation energy is first absorbed by the 4*f*-5*d* transition of Ce³⁺ and transferred to the Gd³⁺ and migrate over the Gd³⁺ lattice to the Tb³⁺, where the energy is released as visible emissions (Boyer et al., 2007; Liu et al., 2009). The visible emission can easily be assigned to transitions between the 4*f* energy levels of the terbium ion. These observations con-

cerning the energy transfer and migration processes in sensitized and activated bulk Gd samples are in good agreement with the published literature reports (Yaiphaba et al., 2010a, 2010b). According to this fluorescence process, the excitation energy is first absorbed by the $4f-5d$ transition of Ce^{3+} and transfer to the Gd^{3+} and migrates over the Gd^{3+} lattice to the Tb^{3+} , where the energy released as fluorescent emissions (Boyer et al., 2007, Yaiphaba et al., 2010a, 2010b).

The emission spectra of all three samples were monitored at 355 nm excitation wavelength in a solid phase at room temperature as shown in Fig. 7. All observed emission peaks of core and core/shell NCs are generated from the $4f-4f$ transitions of Tb ions of $^5D_4 \rightarrow ^7F_6$ (488 nm), $^5D_4 \rightarrow ^7F_5$ (488 nm), $^5D_4 \rightarrow ^7F_5$ (488 nm), $^5D_4 \rightarrow ^7F_4$ (488 nm), $^5D_4 \rightarrow ^7F_3$ (488 nm), $^5D_4 \rightarrow ^7F_2$ (488 nm), and $^5D_4 \rightarrow ^7F_1$ (488 nm), respectively (Ansari and Labis 2012; Ansari et al., 2013). Among the observed emission peaks, the most prominent emission peak is observed at 542 nm ($^5D_4 \rightarrow ^7F_4$), which is known as hypersensitive transition. It is a true fingerprint of characteristic $4f-4f$ emission transitions and provides the chemical bonding information surrounding the terbium ion, which is induced by the change in the chemical environment of Tb ions during formation of a new chemical bond between surface coated $NaGdF_4$ shell and Tb ions. It can be seen in Fig. 7, the emission transitions exhibit inhomogeneous broadening characteristics compared with other Tb doped crystalline materials. It is known that Ce^{3+} is a redox element and shows two oxidation states, in which Ce^{3+} absorbed energy and can be transferred to Ce^{4+} ions. In that case, Ce^{4+} ion is not capable of acting as a sensitizer in this way. To prevent this oxidation, a $NaGdF_4$ layer was developed around the core-NCs. The formed undoped $NaGdF_4$ shell around the core-NCs protect the luminescent center from the surface attached functional groups and quenching sites located at the surface of NCs. For this reason, we formed a shell of $NaGdF_4$. This kind of core/shell structure has been utilized previously by many authors for the similar reason (Boyer et al., 2007; Parchur et al., 2012; Ansari et al., 2014a, 2014b). As seen in Fig. 8, epitaxial growth of a passivated $NaGdF_4$ layer around the luminescent seed core-NCs, a drastic increase in emission intensity is observed in respect to core-NCs. This remarkable increase in emission intensity

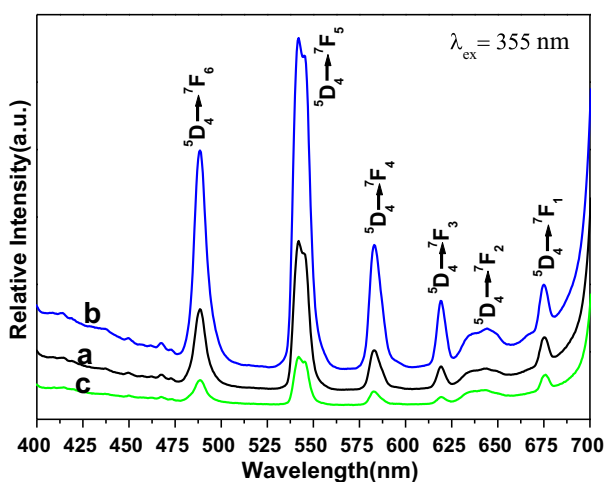


Fig. 7 Emission spectra of (a) core (b) core/shell and (c) core/shell/SiO₂ NCs.

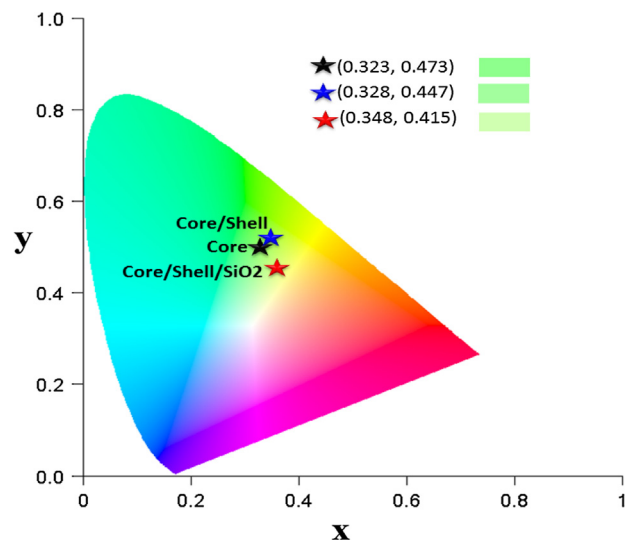


Fig. 8 CIE chromaticity of the core, core/shell and core/shell/SiO₂ NCs.

is attributed to the fact that the $NaGdF_4$ layer protects the core NCs from Ce^{3+} oxidation. It is obvious the formed inert $NaGdF_4$ layer effectively reduce non-radiative quenching of the luminescent lanthanide ions by surface defects and surrounding solvent molecules (Boyer et al., 2007; Ansari et al., 2014a, 2014b). The enhancement of luminescent intensity after growth a shell in respect to core-NCs, it clearly indicates that a layer of undoped $NaGdF_4$ was effectively encapsulated around the core-NCs. Notably, core-NCs are relatively possessing hydrophilic properties, which would indicate that the NCs are dispersed by electrostatic stabilization forces. Although, colloidal stability or hydrophilic nature of the core-NCs is suppressed after surface growth of undoped $NaGdF_4$ layer. The colloidal stability or hydrophilicity of NCs is a crucial parameter for further their use as a luminescent biological tag since the NCs will be exposed with several biological macromolecules. Therefore, the hydrophilicity of the NCs depends on the surface functionalization or coverage groups, which enhanced the solubility character of the nanomaterials. To overcome this problem, we modified the surface of core/shell NCs with amorphous silica. Amorphous silica not only enhanced the colloidal stability or hydrophilicity but also increase the biocompatibility and non-toxicity for further use in biological applications and to maintain the luminescent intensities (Wang et al., 2007; Ansari et al., 2011). It is observed from Figs. 6 and 7, the relatively excitation and emission peak intensity are greatly suppressed after amorphous silica surface modification compared to non-silica modified NCs. The suppression of luminescent intensity caused by grafting of amorphous silica around core-NCs, which have in large amount vibrational modes of silanol (Si-OH) groups, which acts as a luminescence quencher (Wang et al., 2007). This luminescent quencher scattered the emission light and enhanced the non-radiative transition resulting the luminescent intensity is reduced; these observations are consistent with FTIR and UV/Vis results. Whereas, amorphous silica surface modified NCs possess hydrophilic silanol groups, which are highly dispersible in aqueous solvent through electrostatic stabilization forces. These results were strongly supported by previously

published literature reports (Ansari et al., 2011; Ansari et al., 2012; He et al., 2012; Ansari et al., 2014a, 2014b). Fig. 8 illustrates the CIE chromaticity diagram of core and core/shell NCs at 355 nm excitation.

Photoluminescence decay curves of 5D_4 level (545 nm) of Tb^{3+} ion for core, core/shell, and core/shell/SiO₂ NCs under 355 nm excitation is shown in Fig. 9. All the decay curves were measured at room temperature. The decay curve for $^5D_4 \rightarrow ^7F_5$ transition (545 nm) of Tb^{3+} ions are well fitted with monoexponential function as $I = I_0 \exp(-t/\tau_1)$ (Fig. 9), where I_0 and I are the intensities at the $t = 0$ and t ms and τ is the lifetime (1/e lifetime of the emission center) (Parchur et al., 2011; Cao et al., 2014). The fitting parameters obtained after monoexponential fitting are shown in the figure itself. Lifetime values of core particles are slightly higher than core/shell and core/shell/SiO₂ NCs. Core/shell NCs are well fitted on monoexponential decay model ($R^2 = 0.9916$) as compared to core and core/shell/SiO₂ NCs. Furthermore, a biexponential equation which is defined as, $I = I_1 \exp(-t/\tau_1) + I_2 \exp(-t/\tau_2)$, where τ_1 and τ_2 are the fast and slow components of the luminescence lifetime decay constants and I_1 and I_2 are the intensity parameters also used to check the lifetime decay behavior (Parchur et al., 2011). The biexponential fitting to the decay data of core, core/shell, and core/shell/SiO₂ NCs were shown in Fig. S1 and fitting parameters (I_1 , τ_1 , I_2 , τ_2 , τ_{av} and R^2) are summarized in Table S1. Where τ_{av} is the average lifetime for $^5D_4 \rightarrow ^7F_5$ transition of Tb^{3+} ion is calculated using the

formula as $\tau_{av} = (I_1\tau_1 + I_2\tau_2)/(I_1 + I_2)$ (He et al., 2012). There is a slight improvement in R^2 value for core sample whereas no differences were observed for core/shell and core/shell/SiO₂ NCs samples. The τ_{av} values are similar to the values obtained from monoexponential fitting. Biexponential results confirm that the fastest decay component ($I_1(\%)$) changes from 13 to 10% on NaGdF₄ shell coating on core NCs, whereas it is significantly enhanced to 43% on further SiO₂ shell coating on core/shell NCs. For a biexponential fitting, the lifetime decay values for core and core/shell samples are found to be 405 μ s (τ_1) and 5.307 ms (τ_2) with an average lifetime of 4.673 ms (τ_{av}) and core/shell samples 306 μ s (τ_1) and 3.525 ms (τ_2) with an average lifetime of 3.21 ms (τ_{av}), respectively. For core/shell/SiO₂ samples, the lifetime values are found to be 2.24 ms (τ_1) and 4.355 ms (τ_2) with an average lifetime of 3.444 ms (τ_{av}). The τ_1 , τ_2 have a 43 and 57% contribution in τ_{av} value. The different contributions of photoluminescence decay lifetimes arise from several origins. Generally, the fast contribution of a lifetime arises from the exciton, or band-edge emission, an intrinsic semiconductor electron-hole pair recombination process, whereas, the lower lifetime decay arises with traps or surface defects, or dangling bonds located on the surface of nanomaterials (Cheng et al., 2008). Number of dangling bonds present on the nanoparticle will vary depending on the size of the particles, i.e., a decrease in particle size will allow large number of dangling bonds on it and influence the lifetime values (Parchur et al., 2012). It is observed that slower decay component ($I_2(\%)$) slightly increased by $\sim 3\%$ on core/shell formation. Further, SiO₂ shell coating significantly diminishes the $I_2(\%)$ contribution to 57%. This is due to the quenching behavior of luminescence of NCs due to SiO₂ shell formation (Runowski et al., 2013).

The possible cytotoxic response of core NCs with different concentrations (equivalent to 3.12, 6.25, 12.5, 25, 50 and 100

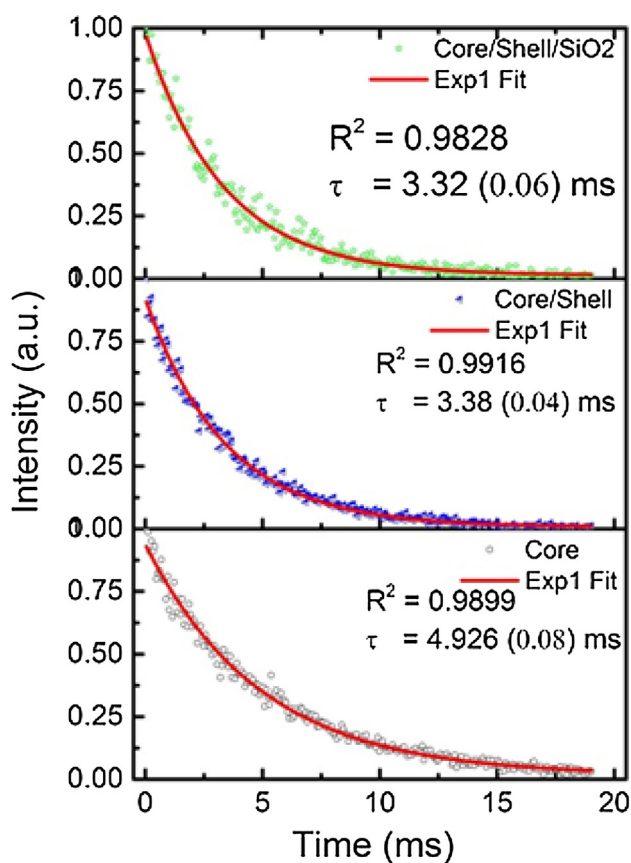


Fig. 9 Photoluminescence decay curves of core, core/shell, and core/shell/SiO₂ NCs at $\lambda_{ex} = 355$ nm and $\lambda_{em} = 541$ nm fitted using monoexponential equations.

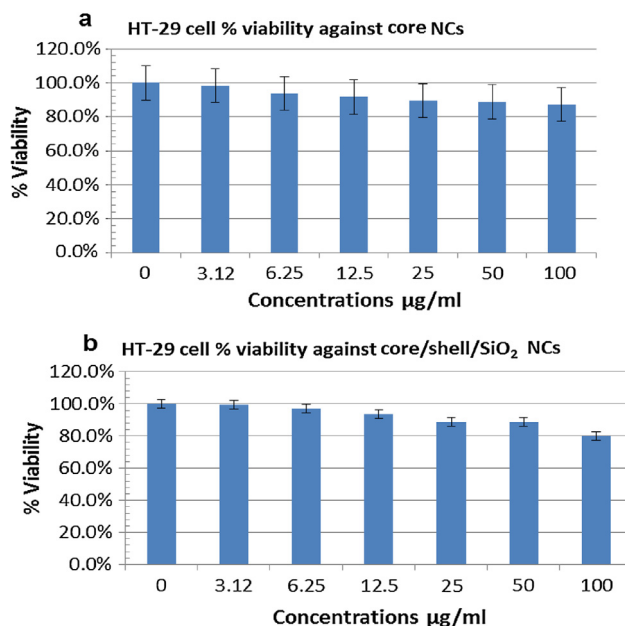
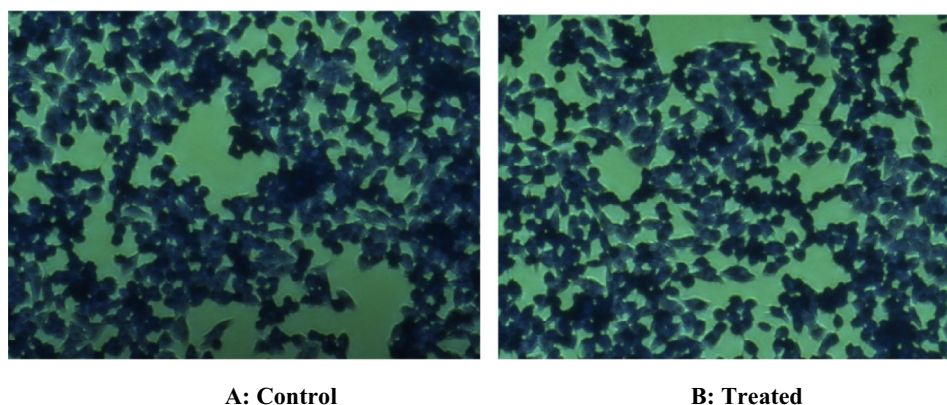


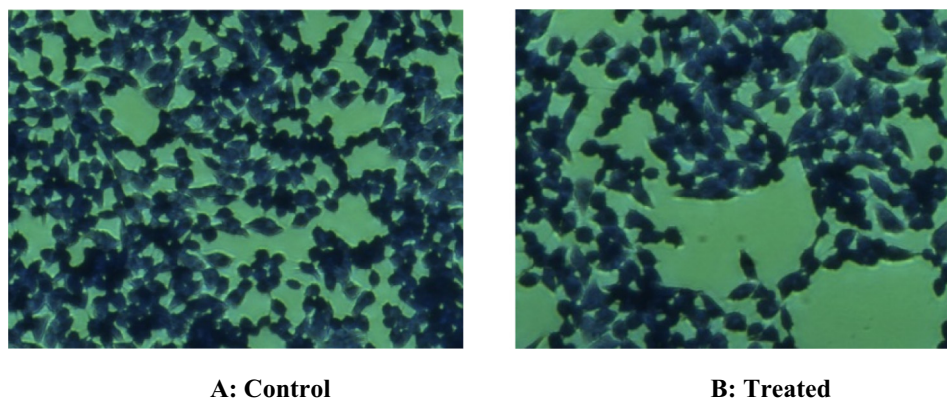
Fig. 10 *In vitro* estimation of the percentage of cell viability in HT-29 cells after exposure to different concentrations of the core (a) and core/shell/SiO₂ NCs (b) for 24 h at 37 °C by MTT assay. Error bars were based on standard deviation of three samples.



A: Control

B: Treated

Fig. 11 Inverted microscope images were illustrating the possible cytotoxic response of core NCs on HT-29 cells through crystal violet staining. (A): No cytotoxicity was observed in control untreated HT29 cells. (B): Nonsignificant cytotoxic response was observed in HT29 exposed with highest (100 μg) concentrations of core NCs. Although very little alterations were observed in morphology and number of HT-29 cells.



A: Control

B: Treated

Fig. 12 Inverted microscope images were illustrating the possible cytotoxic response of core/shell/SiO₂ NCs on HT-29 cells through crystal violet staining. (A): No cytotoxicity was observed in control untreated HT29 cells. (B): Non-significant cytotoxic response was observed in HT29 exposed with highest (100 μg) concentrations of core/shell/SiO₂ NCs. Although little alterations were observed in morphology and number of HT-29 cells.

$\mu\text{g mL}^{-1}$) was assessed on HT-29 cells through the MTT reducing assay. The dose-dependent response of core NCs on the viability of HT-29 cell on 24 h exposure was evaluated with respect to the control group (no test NCs) (Fig. S2). The results illustrate that HT-29 cell viability remains 90–98 % with all examined concentrations. The HT-29 cells survive showed about 90 % of cell viability towards highest concentration (100 $\mu\text{g mL}^{-1}$) of core NCs (Fig. 10a), showing the less cytotoxicity and good biocompatibility of test sample for their application in biomedical science such as diagnostic and imaging. Similarly, we assessed the cytotoxic response of core/shell/SiO₂ NCs on the viability of growing HT-29 cell line using different concentrations (equivalent to 3.12, 6.25, 12.5, 25, 50 and 100 $\mu\text{g mL}^{-1}$) by MTT reduction assay. In the case of core NCs the dose-dependent response on the viability of HT-29 cell on 24 h exposure was also evaluated with respect to the control group (no test NCs) (Fig. S3). The results illustrate that HT-29 cell viability remains 81–97 % with different examined concentrations. The HT-29 cells survive showed about 81 % of cell viability towards highest concentration (100 $\mu\text{g mL}$

$^{-1}$) of core/shell/SiO₂ NCs (Fig. 10b), showing the less cytotoxicity and good biocompatibility of test sample for their application in biomedical science such as diagnostic and imaging. The results of control drugs towards HT-29 cells corroborate with our previous published (here data not shown) study (Khan et al., 2016a, 2016b). Moreover, the core/shell and core/shell/SiO₂ NCs demonstrated the non-significant value of IC₅₀ comparing to free doxorubicin against HT-29 cells. The control drug doxorubicin showed the value of about IC₅₀ 11 $\mu\text{g/mL}$ as publish in our recent report.

Fig. 11(A and B) shows the results of exposure of core NCs in inverted microscopy. The results illustrate the non-significant effect of core NCs on growing HT-29 cells with 100 μg concentration. Also, the less-significant cytotoxic response of core/shell/SiO₂ NCs with 100 μg (highest) concentration were observed on treating HT-29 cells with respect to untreated control cells (Fig. 12A and B). These results showed less cytotoxicity of synthesized NCs as non-significant change on the shape change of the HT-29 cells which was in according to the our MTT assay results. The inverted microscopy images

confirmed that core/shell/SiO₂ NCs entered more efficiently than core NCs into HT-29 cells.

4. Conclusions

In summary, we have designed and prepared NaGdF₄:Ce/Tb (core), NaGdF₄:Ce/Tb@NaGdF₄(core/shell) and NaGdF₄:Ce/Tb@NaGdF₄@SiO₂ (core/shell/SiO₂) NCs that exhibits intensive green emission under UV excitation and form colloidal solution in aqueous solvent. Comparative spectral results of core, core/shell and silica modified core/shell/SiO₂ NCs demonstrated a size based alteration in optical properties and exhibited higher quantum efficiency under ultraviolet light and a greater resistance to cerium oxidation when compared to the core-NCs. Our findings suggest that morphological and optical (absorption, band gap, excitation, emission, lifetime, etc.) properties of the designed materials were affected after shell formation around the core NCs. It can be seen the luminescent intensity of core NCs was greatly enhanced in core/shell nanostructures. This large luminescent enhancement is proposed to originate from a modification of the crystal structure of NaGdF₄ and an improvement in the crystallinity of the core/shell nanophase. According to the *in vitro* cytotoxicity results, the core/shell/SiO₂ NCs showed excellent biocompatibility and non-toxicity than their respective core NCs, it indicated that silica surface modification enhanced their biocompatibility and non-toxicity character, which is also easily available for conjugation with bio-macromolecules for bio-labeling/bio-probe, etc. Moreover, high entering efficiency of core/shell/SiO₂ NCs in HT-29 showed their implication in the biomedical field for diagnosis and imaging of cancer in early stages. The results confirmed that core/shell/SiO₂ NCs are highly promising candidates for future photonic based bio-applications such as biomarker/optical bio-probe/ bio-detection and biolabeling, etc.

Acknowledgment

The author is thankful for the financial support to the King Abdullah Institute for Nanotechnology, Deanship of Scientific Research, King Saud University, Riyadh, Saudi Arabia.

Appendix A. Supplementary material

Supplementary data associated with this article can be found, in the online version, at <https://doi.org/10.1016/j.arabjc.2017.10.008>.

References

- Alivisatos, P., 2004. The use of nanocrystals in biological detection. *Nat. Biotechnol.* 22 (1), 47–52.
- Ansari, A.A., Alam, M., et al, 2011. Luminescent mesoporous LaVO₄:Eu³⁺ core-shell nanoparticles: synthesis, characterization, biocompatibility and their cytotoxicity. *J. Mater. Chem.* 21 (48), 19310–19316.
- Ansari, A.A., Hasan, T.N., et al, 2013. In-vitro cyto-toxicity, genotoxicity, and bio-imaging evaluation of one-pot synthesized luminescent functionalized mesoporous SiO₂@Eu(OH)₃ core-shell microspheres. *Nanomed.-Nanotech. Biol. Med.* 9 (8), 1328–1335.
- Ansari, A.A., Labis, J.P., 2012. One-pot synthesis and photoluminescence properties of luminescent functionalized mesoporous SiO₂@Tb(OH)₃ core-shell nanospheres. *J. Mater. Chem.* 22 (32), 16649–16656.
- Ansari, A.A., Parchur, A.K., et al, 2014a. Effect of surface coating on optical properties of Eu³⁺-doped CaMoO₄ nanoparticles. *Spectrochimica Acta Part a-Mole. Biomole. Spectroscop.* 131, 30–36.
- Ansari, A.A., Parchur, A.K., et al, 2014b. Influence of surface coating on structural and photoluminescent properties of CaMoO₄:Pr Nanoparticles. *Journal of Fluorescence* 24 (4), 1253–1262.
- Ansari, A.A., Singh, S.P., et al, 2012. Synthesis of optically active silica-coated NdF₃ core-shell nanoparticles. *Spectrochim. Acta Part a-Mole. Biomole. Spectroscop.* 86, 432–436.
- Ansari, A.A., Yadav, R., et al, 2016. Enhanced luminescence efficiency of aqueous dispersible NaYF₄:Yb/Er nanoparticles and the effect of surface coating. *Rsc Adv.* 6 (26), 22074–22082.
- Bao, Y., Luu, Q.A.N., et al, 2012. Upconversion polymeric nanofibers containing lanthanide-doped nanoparticles via electrospinning. *Nanoscale* 4 (23), 7369–7375.
- Boyer, J.C., Gagnon, J., et al, 2007. Synthesis, characterization, and spectroscopy of NaGdF₄:Ce³⁺, Tb³⁺/NaYF₄ core/shell nanoparticles. *Chem. Mater.* 19 (14), 3358–3360.
- Cao, C.Y., Guo, S.L., et al, 2014. Luminescent Properties of NaGdF₄:Ln(3+) (Ln(3+) = Ce³⁺, Tb³⁺) Phosphors. *J. Nanosci. Nanotechnol.* 14 (5), 3735–3738.
- Cheng, K.H., Aijmo, J., et al, 2008. Luminescence decay dynamics and trace biomaterials detection potential of surface-functionalized nanoparticles. *J. Phys. Chem. C* 112 (46), 17931–17939.
- Cui, S.S., Chen, H.Y., et al, 2012. Amphiphilic chitosan modified upconversion nanoparticles for in vivo photodynamic therapy induced by near-infrared light. *J. Mater. Chem.* 22 (11), 4861–4873.
- Dhanaraj, J., Jagannathan, R., et al, 2001. Photoluminescence characteristics of Y₂O₃:Eu³⁺ nanophosphors prepared using sol-gel thermolysis. *J. Phys. Chem. B* 105 (45), 11098–11105.
- Gao, G. J., A. Winterstein-Beckmann, et al., (2015). “Faraday rotation and photoluminescence in heavily Tb³⁺-doped GeO₂-B₂O₃-Al₂O₃-Ga₂O₃ glasses for fiber-integrated magneto-optics.” *Scientific Reports* 5.
- Goldys, E.M., Drozdowicz-Tomsia, K., et al, 2006. Optical characterization of Eu-doped and undoped Gd₂O₃ nanoparticles synthesized by the hydrogen flame pyrolysis method. *J. Am. Chem. Soc.* 128 (45), 14498–14505.
- He, M., Huang, P., et al, 2012. “Phase- and size-controllable synthesis of hexagonal upconversion rare-earth fluoride nanocrystals through an oleic acid/ionic liquid two-phase system. *Chem. – A Europ. J.* 18 (19), 5954–5969.
- Huhtinen, P., Kivelä, M., et al, 2005. Synthesis, characterization, and application of Eu(III), Tb(III), Sm(III), and Dy(III) lanthanide chelate nanoparticle labels. *Anal. Chem.* 77 (8), 2643–2648.
- Kang, X.J., Cheng, Z.Y., et al, 2011. Core-shell structured upconversion luminescent and mesoporous NaYF₄:Yb³⁺/Er³⁺@nSiO₂@mSiO₂ Nanospheres as carriers for drug delivery. *J. Phys. Chem. C* 115 (32), 15801–15811.
- Kar, A., Kundu, S., et al, 2015. Lanthanide-doped nanocrystals: strategies for improving the efficiency of upconversion emission and their physical understanding. *Chemphyschem* 16 (3), 505–521.
- Khan, S., Ansari, A.A., et al, 2016a. In vitro evaluation of anticancer and biological activities of synthesized manganese oxide nanoparticles. *Medchemcomm* 7 (8), 1647–1653.
- Khan, S., Ansari, A.A., et al, 2015. In vitro evaluation of anticancer and antibacterial activities of cobalt oxide nanoparticles. *J. Biol. Inorg. Chem.* 20 (8), 1319–1326.
- Khan, S., Ansari, A.A., et al, 2016b. Design, synthesis and in vitro evaluation of anticancer and antibacterial potential of surface modified Tb(OH)₃@SiO₂ core-shell nanoparticles. *Rsc Advances* 6 (22), 18667–18677.
- Liu, C.H., Wang, H., et al, 2009. Morphology- and phase-controlled synthesis of monodisperse lanthanide-doped NaGdF₄ nanocrystals with multicolor photoluminescence. *J. Mater. Chem.* 19 (4), 489–496.

- Liu, T.C., Liu, B.S., et al, 2005. The fluorescence bioassay platforms on quantum dots nanoparticles. *J. Fluorescence* 15 (5), 729–733.
- Parchur, A.K., Ningthoujam, R.S., et al, 2011. Luminescence properties of Eu^{3+} doped CaMoO_4 nanoparticles. *Dalton Trans.* 40 (29), 7595–7601.
- Parchur, A.K., Prasad, A.I., et al, 2012. Luminescence properties of Tb^{3+} -doped CaMoO_4 nanoparticles: annealing effect, polar medium dispersible, polymer film and core-shell formation. *Dalton Trans.* 41 (36), 11032–11045.
- Prorok, K., Bednarkiewicz, A., et al, 2014. The impact of shell host ($\text{NaYF}_4/\text{CaF}_2$) and shell deposition methods on the up-conversion enhancement in Tb^{3+} , Yb^{3+} codoped colloidal alpha- NaYF_4 core-shell nanoparticles. *Nanoscale* 6 (3), 1855–1864.
- Reiss, P., Protière, M., et al, 2009. Core/shell semiconductor nanocrystals. *Small* 5 (2), 154–168.
- Riwotzki, K., Meyssamy, H., et al, 2000. Liquid-phase synthesis of doped nanoparticles: colloids of luminescing LaPO_4 : Eu and CePO_4 : Tb particles with a narrow particle size distribution. *J. Phys. Chem. B* 104 (13), 2824–2828.
- Runowski, M., Dabrowska, K., et al, 2013. Core/shell-type nanorods of Tb^{3+} -doped LaPO_4 , modified with amine groups, revealing reduced cytotoxicity. *J. Nanopart. Res.* 15 (11).
- Tauc, J., Menth, A., 1972. States in the gap. *J. Non-Cryst. Solids* 8, 569–585.
- Vetrone, F., Naccache, R., et al, 2009. The active-core/active-shell approach: a strategy to enhance the upconversion luminescence in lanthanide-doped nanoparticles. *Adv. Func. Mater.* 19 (18), 2924–2929.
- Wang, F., Deng, R.R., et al, 2011. Tuning upconversion through energy migration in core-shell nanoparticles. *Nat. Mater.* 10 (12), 968–973.
- Wang, F., Fan, X.P., et al, 2007. Multicolour $\text{PEI}/\text{NaGdF}_4$: Ce^{3+} , Ln ($3+$) nanocrystals by single-wavelength excitation. *Nanotechnology* 18 (2).
- Wang, Z.L., Quan, Z.W., et al, 2006. Facile synthesis and photoluminescent properties of redispersible CeF_3 , CeF_3 : Tb^{3+} , and CeF_3 : $\text{Tb}^{3+}/\text{LaF}_3$ (core/shell) nanoparticles. *Chem. Mater.* 18 (8), 2030–2037.
- Xu, W., Zhu, Y.S., et al, 2013. A novel strategy for improving upconversion luminescence of NaYF_4 :Yb, Er nanocrystals by coupling with hybrids of silver plasmon nanostructures and poly (methyl methacrylate) photonic crystals. *Nano Res.* 6 (11), 795–807.
- Yaiphaba, N., Ningthoujam, R.S., et al, 2010a. Luminescence properties of redispersible Tb^{3+} -Doped GdPO_4 nanoparticles prepared by an ethylene glycol route. *Eur. J. Inorg. Chem.* (18), 2682–2687.
- Yaiphaba, N., Ningthoujam, R.S., et al, 2010b. Luminescence, lifetime, and quantum yield studies of redispersible Eu^{3+} -doped GdPO_4 crystalline nanoneedles: core-shell and concentration effects. *J. Appl. Phys.* 107 (3).
- Zhang, Y.W., Sun, X., et al, 2005. Single-crystalline and monodisperse LaF_3 triangular nanoplates from a single-source precursor. *J. Am. Chem. Soc.* 127 (10), 3260–3261.